

## ARTICLE OPEN



# Ultra-high temperature tolerant flexible transparent electrode with embedded silver nanowires bundle micromesh for electrical heater

Bowen Sun<sup>1</sup>, Ruixue Xu<sup>1</sup>, Xu Han<sup>1</sup>, Jing Xu<sup>1</sup>, Wang Hong<sup>1</sup>, Yimeng Xu<sup>1</sup>, Zhiwei Fu<sup>1</sup>, He Zhu<sup>1</sup>, Xin Sun<sup>1</sup>, Jiangxin Wang<sup>2</sup>, Peng Cui<sup>3</sup>, Jingjing Chang<sup>4</sup>✉, Jiaqing Xiong<sup>5</sup>✉ and Kai Qian<sup>1,6,7</sup>✉

To realize high performance flexible transparent electronics with extreme environmental adaptivity, Ag nanowires (Ag NWs) electrodes should simultaneously meet the requirements of high-temperature tolerance, chemical and mechanical robustness. Herein, a scalable Ag NWs bundle micro-meshes embedded in polyimide (Ag BMs/ePI) conducting film *via* a facile spray coating and transfer method is reported. Due to the synergistic effect of bundle micromesh and embedded architecture, the Ag BMs/ePI electrode exhibits high thermal stability (370 °C and 400 °C under ambient and nitrogen atmosphere conditions, respectively), low sheet resistance variation (<4%), good corrosion and deformation resistance. As an electrical heater, the Ag BMs/ePI can achieve ~204 °C with the fast thermal response time of ~8 s at 8 V, and exhibits good heating stability under bent condition. This work offers a promising platform for the emerging flexible transparent electronics to adapt extreme environments, especially for those devices which require high-temperature processing.

*npj Flexible Electronics* (2022)6:48; <https://doi.org/10.1038/s41528-022-00182-8>

## INTRODUCTION

Flexible transparent conductors pervade numerous modern technologies of optoelectronic devices<sup>1–4</sup>, and due to the desirable electrical, optical, and mechanical properties, flexible transparent metal nanowires electrodes (e.g., Cu NWs, Ag NWs, Au NWs) are being explored for many different applications, such as interactive electronics, heaters, solar cells, electrochromic devices, and so on<sup>5–15</sup>. As a cost-effective alternative to the Ag NWs electrode, Cu NWs have nearly the same conductivity as Ag NWs, which have attracted a great concern with the advantage of considerably cheaper than Ag<sup>12,13,15</sup>. However, the sensitivity to water and oxygen now is the main obstacle for the stable conductivity of Cu NWs in various of applications<sup>11</sup>. For the inert Au NWs electrode, it is hindered by the extortionate price of Au. Considering the comprehensive situation, the Ag NWs become the most potential material in the flexible transparent electrode. In real applications, the Ag NWs electrodes usually suffer from various extreme environments, such as high temperature, chemical erosion, and mechanical deformation. Of which, the thermal stability of Ag NWs electrode is one of the ungently desired performances for typical optoelectronic device fabrication with high-temperature annealing process<sup>16–19</sup>, and more importantly these electrodes are frequently heated up due to Joule heating<sup>20</sup>. However, due to the inherent drawback of thermally activated Rayleigh instability, the surface diffusion of Ag atoms in Ag NWs would result in spheroidization and discontinuous networks, which renders a decreased lifetime to restrict the capability of Ag NWs conductor for potential applications<sup>21–24</sup>.

To address the thermal stability issue of Ag NWs electrode for their wide applications, efforts have been made to develop surface passivation technologies using organic, inorganic, or carbon-

based materials. For instance, the Ag NWs electrode embedded in glass-fabric reinforced composite can withstand the temperature of ~250 °C for 2 h<sup>25</sup>. Graphene can dissipate heat energy and provide moisture protection to safeguard Ag NWs electrode, which was able to maintain stability at 300 °C<sup>26</sup>. In addition, inorganic capping layers (e.g., ZnO, TiO<sub>2</sub>) with a high melting temperature were also proposed for Ag NWs encapsulation<sup>6,27</sup>, where the conducting film can withstand thermal processing at ~300 °C with little change in sheet resistance. Nevertheless, these preparation processes are complicated and costly to improve the thermal stability of the conducting Ag NWs films. In addition, from a technical point of view, the high performance flexible transparent Ag NWs electrode should also satisfy concurrently other key requirements, such as uniform sheet resistance ( $R_s$ ), mechanical robustness and electrical durability in the harsh environment, smooth surface topography (~a few nanometers are preferred), and strong adhesion with the substrate. However, a solution simultaneously resolving the afore-mentioned problems with the Ag NWs conductors has not surfaced and is an urgent challenge. On the other hand, the metal nanowire-based networks electrodes always suffer from the large junction resistance between nanowires<sup>22,28</sup>. Therefore, various techniques such as regular thermal annealing<sup>23,29</sup>, laser nano-welding<sup>30</sup>, flash lamp welding<sup>31</sup>, chemical treatment<sup>32</sup>, mechanical welding<sup>33</sup> and electrical annealing<sup>21,34</sup> are always required to improve the metal nanowires nano-welding to lower the junction resistance, where these processes may increase manufacturing cost or be complicated. These problems motivate the search for strategies to facilely prepare the high performance flexible transparent Ag NWs electrode.

<sup>1</sup>School of Microelectronics, Shandong Technology Center of Nanodevices and Integration, Shandong University, Jinan 250100, China. <sup>2</sup>School of Mechanical Engineering, Sichuan University, Chengdu 610041, China. <sup>3</sup>Key Lab for Special Functional Materials of Ministry of Education, School of Materials Science and Engineering, Henan University, Kaifeng 475004, China. <sup>4</sup>State Key Discipline Laboratory of Wide Band Gap Semiconductor Technology, Shaanxi Joint Key Laboratory of Graphene, School of Microelectronics, Xidian University, 2 South Taibai Road, Xi'an 710071, China. <sup>5</sup>Innovation Center for Textile Science and Technology, Donghua University, Shanghai 201620, China. <sup>6</sup>State Key Laboratory of Crystal Materials, Shandong University, Jinan 250100, China. <sup>7</sup>Shenzhen Research Institute of Shandong University, Shenzhen 518057, China. ✉email: [jjingchang@xidian.edu.cn](mailto:jjingchang@xidian.edu.cn); [jqiong@dhu.edu.cn](mailto:jqiong@dhu.edu.cn); [kaiqian@sdu.edu.cn](mailto:kaiqian@sdu.edu.cn)

Previously, we demonstrated a spray-assisted self-assembly method to prepare Ag NWs conducting film on ethyl cellulose (EC) substrate<sup>7</sup>, opening a route for scalable production of Ag NWs electrode with good optoelectrical properties. Especially, compared with random Ag NWs networks electrode, the Ag BMs electrode can achieve a higher conductivity with a smaller number of nanowires due to the explicit conductive paths of Ag NWs bundles. It is worth noting that the solvents, substrate surface tensions, and aspect ratios of Ag NWs will determine nanowires assembly to affect the Ag BMs morphology, which have a great impact on the capillary flow and Marangoni reflux. For example, solvents with different evaporation rates would produce different driving forces from coffee-ring effect, leading to diverse assembly behaviors due to the different aspect ratios of Ag NWs. In addition, there are also some other approaches to prepare the Ag NW bundled network electrodes with assistance of template such as leaf skeletons<sup>35</sup> and random crack mold<sup>36</sup>. As a comparison, the Ag BMs electrode preparation with spray-assisted self-assembly method does not require template, of which structure is easy to be tuned *via* controlling the spraying velocity and Ag NWs dimension<sup>7,37</sup>. However, the Ag NWs/EC conductor is severely restricted for practical applications due to the poor thermal and chemical stabilities. Here, we present a facile spray coating and transfer method to prepare high performance Ag NWs bundle micromeshes (Ag BMs) electrode embedded in the heat-resistant polyimide (PI) substrate (i.e., Ag BMs/ePI), which exhibits high-temperature tolerance (400 °C at N<sub>2</sub> atmosphere and 370 °C in ambient atmosphere for at least 1 h), long time stability in ambient atmosphere ( $\Delta R/R_0 < 5\%$  after exposure to air for 8 months), remarkable mechanical flexibility under bending stress ( $\Delta R/R_0 < 2\%$  after 10,000 cycles with bending radius  $r = 1.5$  mm), good resistance to organic solvent (acetone, isopropanol, ethanol, toluene), acid (pH = 1.0) and alkaline (pH = 12.0) solutions, good optoelectronic performances with uniform sheet resistance distribution ( $R_s \sim 10 \pm 0.4$  ohm sq<sup>-1</sup>), low surface roughness (RMS,  $4.57 \pm 2.42$  nm) as well as reliable adhesion between Ag BMs and PI substrate ( $\Delta R/R_0 < 1\%$  after 1000 cycles of adhesion test). As a proof of concept, the Ag BMs/ePI films are employed to construct flexible transparent heaters, which show extraordinary mechanical robustness and exceptional heating performance with rapid response time, high saturation temperature up to 204 °C with the voltage of 8 V, good heating repeatability, stability, and reliability owing to the advantage of Ag NWs bundle micromesh construction and embedded structure protected by the densely wrapped polyimide matrix.

## RESULTS AND DISCUSSION

### Preparation and characterization of Ag BMs/ePI electrodes

Flexible transparent Ag BMs/ePI conducting film fabrication was schematically illustrated in Fig. 1a. First, the Ag BMs was prepared via spray-assisted self-assembly technique on polydimethylsiloxane (PDMS) substrate due to the instantaneous scalable coffee-ring effect occurred in the sprayed droplets<sup>7,37</sup>, then PI solution was spin-coated on the Ag BMs surface and hence densely wrapped the Ag NWs. After the thermal annealing process, the Ag BMs embedded in PI matrix (Ag BMs/ePI) electrode can be easily peeled off from the substrate, where the Ag BMs were partially embedded in the polyimide film with conformal encapsulation. As shown in Fig. 1b–e and Supplementary Fig. 1a–d, the Ag BMs inlaid uniformly and regularly in PI matrix, leading to uniform sheet resistance distribution. As a typical example, Fig. 1f and Supplementary Fig. 2 presented the Ag BMs/ePI electrode (10 cm × 10 cm) with quite uniform  $R_s$  of  $10 \pm 0.4$  ohm sq<sup>-1</sup> (~4% variation in sheet resistance). This electrical homogeneity of Ag BMs/ePI electrode, which has a substantial influence on device overall performance, is better than that of high-quality commercial

flexible ITO film (11.2%)<sup>38</sup>. The transmittance, sheet resistance and haze of the Ag BMs/ePI electrode can be easily tuned by controlling the Ag NWs amount for different applications (Fig. 1g and Supplementary Fig. 3a). A representative Ag BMs/ePI electrode with sheet resistance of  $\sim 30$  ohm sq<sup>-1</sup>, 80.14% transmittance in the visible range, and low haze of 5.4% was attained. The intrinsic roughness of Ag NWs electrode resulted from the nanowires percolation or stacking, which might render short circuit and device failure. Low surface roughness of Ag NWs electrode is important for stable integration of many flexible and transparent electronic devices. Unlike the highly coarse Ag BMs on substrate surface (Supplementary Fig. 3b–e), a flat and solid conducting surface was obtained by embedding the Ag BMs in the PI substrate (Fig. 1h). The surface roughness (RMS) was significantly reduced from  $43 \pm 4.6$  nm of Ag BMs on substrate surface (Supplementary Fig. 3b–e) to  $4.57 \pm 2.42$  nm for Ag BMs/ePI (Fig. 1h). Moreover, compared with the original  $R_s$  of Ag BMs on the donor PDMS substrate, there was a slightly decreased  $R_s$  for Ag BMs/ePI electrode due to the tightening effect and improved nanowire-nanowire contacts endowed by the curing process of PI matrix (Supplementary Fig. 3f). This facile solution spray coating and transfer method can easily realize low-cost, high-speed, and roll-to-roll manufacturing for flexible transparent electrode with simple equipment, which is favorable to industrial applications.

### Stability of Ag BMs/ePI electrodes

As mentioned before, to guarantee high device yield and performance, the flexible transparent Ag NWs electrodes are supposed to sustain high temperature in manufacturing and post-processing steps. The high thermal stability of the Ag BMs/ePI was evaluated by directly measuring  $R_s$ , where the samples were placed in tubular furnace at ambient and N<sub>2</sub> atmosphere conditions, respectively. For the Ag BMs/ePI electrode ( $R_s \sim 10$  ohm sq<sup>-1</sup>), there was almost no sheet resistance change after 2 h at 350 °C (Fig. 2a) in an ambient atmosphere. Most notably, it was capable of withstanding thermal processing at high temperature of 350 °C and 400 °C for at least 10 h and 1 h under N<sub>2</sub> atmosphere with little change in sheet resistance (Fig. 2a, b, Supplementary Fig. 4a), which would pave the way for Ag NWs-based electronics application in high temperature. This high-temperature tolerance of Ag BMs/ePI electrode is comparable or superior to other selected important works on improving the thermal stability of Ag NWs by use of surface passivation technologies (Supplementary Fig. 4b). With the temperature and annealing time increase, Ag atomic diffusion in Ag NWs is increased, and kinetic limitations to reconstruction are therefore more easily overcome<sup>20</sup>. Hence, the spheroidization phenomena of Ag NWs (Supplementary Fig. 4c) would deteriorate greatly with the increase of annealing temperature and time, leading to the electrical failure of Ag NWs electrode. The stability of Ag BMs/ePI electrode in air is less than in nitrogen resulted from the atmospheric corrosion (e.g., sulfidation, oxidation), leading to accelerated failure of Ag NWs. As a comparison, for the random Ag NWs networks (Ag RNs) on substrate surface, there is always a sharp rise in sheet resistance below 200 °C due to the coalescence of the nanowires into discrete nanoparticles<sup>18,22–24,39</sup>. To further quantitatively analyze the efficacy of the embedded bundle micromesh structure for high-temperature tolerance, the sheet resistance was evaluated and compared with random Ag NWs networks on PI surface (Ag RNs/Pis) as a function of the annealing temperature to highlight the high-temperature tolerance of Ag BMs/ePI electrode. As shown in Fig. 2c, Ag RNs/Pis and Ag BMs/ePI electrodes were heated in air and N<sub>2</sub> atmosphere conditions for 1 h at different temperatures. In the case of the Ag RNs/Pis electrode, an increase in sheet resistance began at 160 (in air) and 170 °C (in N<sub>2</sub>), while the  $R_s$  increased slightly at 370 °C (in air) and 400 °C (in N<sub>2</sub>) for Ag BMs/ePI electrode, respectively. For this significant improvement of Ag BMs/ePI electrode against high temperature, it is attributed to the structural morphology of the Ag

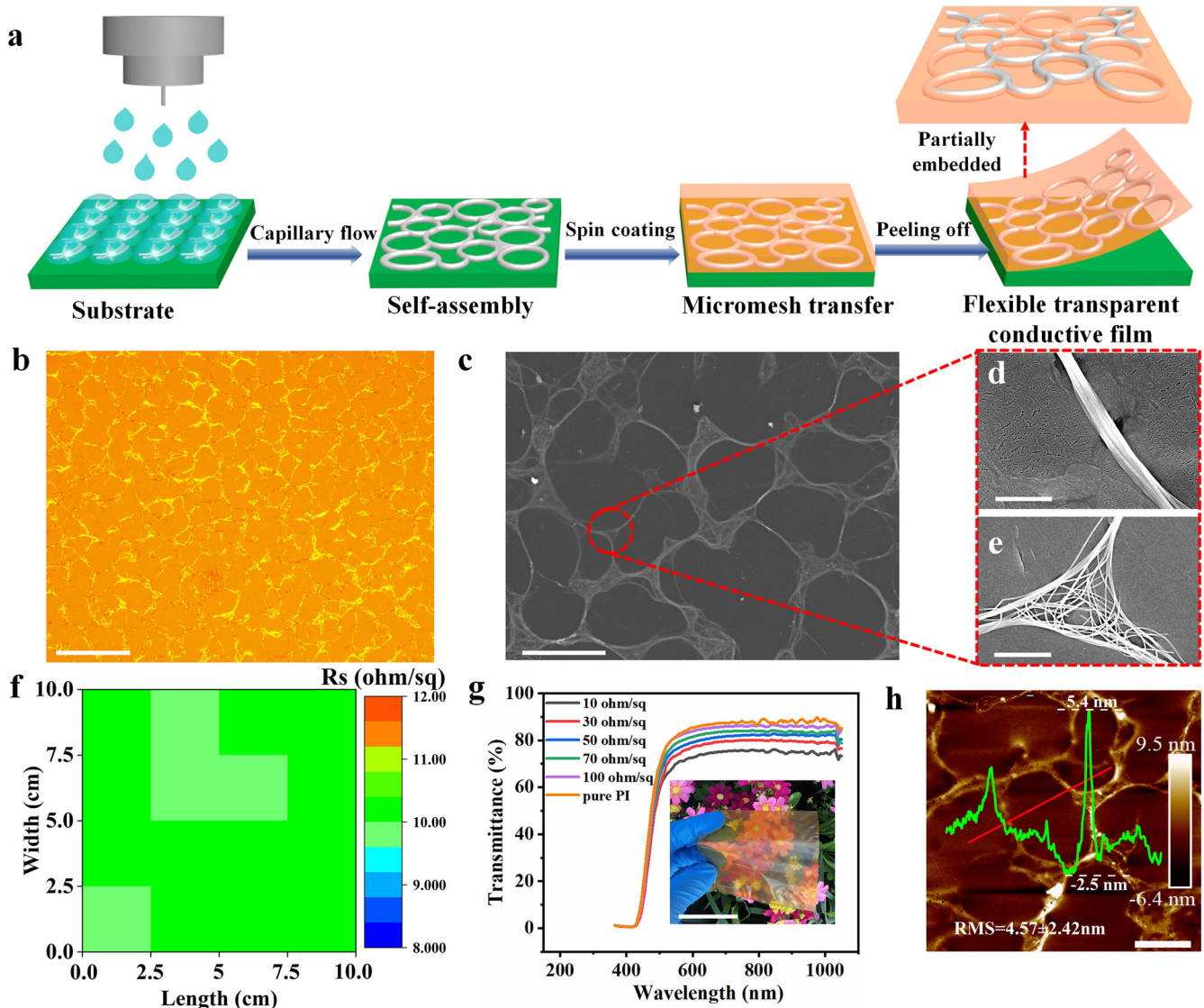


**Fig. 1 Fabrication and general morphology.** **a** Schematic illustration of the fabrication process for Ag NWs bundle micromeshes (Ag BMs) electrode embedded in PI matrix, i.e., Ag BMs/ePI. **b** Optical micrograph of Ag BMs/ePI electrode ( $\sim 10 \text{ ohm sq}^{-1}$ ), indicating uniform Ag BMs distribution. Scale bar was  $50 \mu\text{m}$ . **c** SEM image of the Ag BMs/ePI electrode (scale bar was  $20 \mu\text{m}$ ), corresponding to typical bundle **d** and knot **e** morphology. The scale bars in **d** and **e** were  $3 \mu\text{m}$ . **f** The sheet resistance of Ag BMs/ePI electrode at different positions, indicating highly uniform distribution. The real  $R_s$  values were exhibited in Supplementary Fig. 2. **g** Transmittance spectra of Ag BMs/ePI electrode with different sheet resistance. The inset photo is  $10 \text{ cm} \times 10 \text{ cm}$  flexible transparent Ag BMs/ePI electrode. Scale bar was  $5 \text{ cm}$ . **h** AFM image of Ag BMs/ePI electrode ( $\sim 10 \text{ ohm sq}^{-1}$ ) for low surface roughness demonstration. Scale bar was  $10 \mu\text{m}$ .

NWs (Fig. 2d). That is, the enhanced thermal stability of Ag BMs/ePI electrode was endowed by the embedded structure and bundle micromesh construction of Ag NWs.

To clarify the high-temperature tolerance property conferred by the embedded structure, the Ag NWs electrode ( $R_s \sim 10 \text{ ohm sq}^{-1}$ ) formed on PI surface was measured as a control. The Ag BMs on PI surface (i.e., Ag BMs/PIs) ended up with severe degradation of the electrical performance at lower temperature of  $240^\circ\text{C}$  in air and  $265^\circ\text{C}$  in  $\text{N}_2$  after 30 min (Fig. 2e). While there was a great improvement on the thermal stability of the Ag BMs/ePI electrode, which can maintain stable electrical property at  $350^\circ\text{C}$  in air and  $\text{N}_2$  atmosphere conditions for  $\sim 2 \text{ h}$  (Fig. 2a) and  $\sim 15 \text{ h}$  (Supplementary Fig. 4a), respectively. For the random Ag NWs networks (Ag RNs), the Ag RNs embedded in PI matrix (Ag RNs/ePI) electrode also exhibited higher thermal stability than Ag RNs on PI surface (Ag RNs/PIs) electrode (Fig. 2a, e). The high-temperature durability of Ag NWs electrodes with embedded structure stems

from the fact that the Ag NWs are well protected by the thermal stable PI matrix. During transfer process, the PI solution would adsorb strongly on Ag NWs and provide optimally conformal encapsulation, leaving the minimal surface opening of Ag NWs for electrical conduction. For Ag NWs under thermal stress, the surface diffusion of Ag atoms will be accelerated in view of the high surface-to-volume ratio, leading to unstable Ag NWs electrode<sup>20</sup>. In this work, the encapsulation with PI matrix would effectively suppress the Ag atoms diffusion in nanowire surface to prevent disconnection of Ag NWs, thereby enhancing the temperature tolerance of Ag NWs with the embedded structure.

On the one hand, to verify the enhanced thermal stability of Ag NWs electrodes endowed by the bundle micromesh construction, Ag BMs and reference sample of Ag RNs electrodes were annealed under ambient and  $\text{N}_2$  atmospheres for comparison (Fig. 2e). The Ag BMs/PIs was more stable against high temperature (Fig. 2e), of which sheet resistance increased after  $\sim 30 \text{ min}$  at  $240^\circ\text{C}$  (ambient

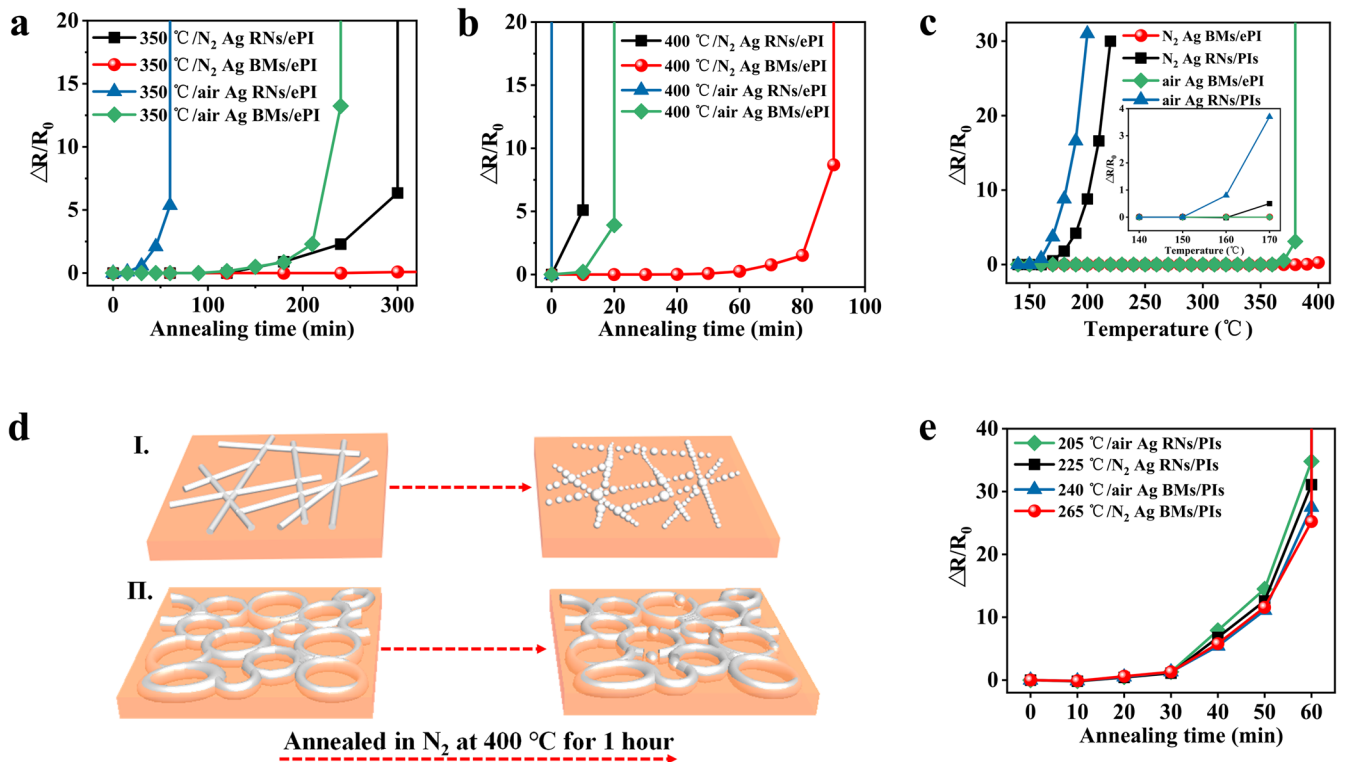


**Fig. 2 Thermal stability of the Ag NWs electrode with  $R_s$  of  $\sim 10 \text{ ohm sq}^{-1}$ .** **a**  $\Delta R/R_0$  vs. annealing time for Ag BMs/ePI and random Ag NWs networks embedded in PI (Ag RNs/ePI) annealed at 350 °C in air and  $N_2$  atmosphere, respectively. **b**  $\Delta R/R_0$  vs. annealing time for Ag BMs/ePI and Ag RNs/ePI annealed at 400 °C in air and  $N_2$  atmosphere, respectively. **c**  $\Delta R/R_0$  vs. annealing temperature for random Ag NWs networks on PI surface (Ag RNs/PIs) and Ag BMs/ePI in air and  $N_2$  atmosphere, respectively. Each sample was heated for 1 h with temperature gradient of 10 °C. **d** The schematic diagram for morphological evolution of Ag NWs at temperature of 400 °C in  $N_2$  atmosphere, where the spheroidization occurred for the random Ag NWs networks on PI surface (i), while the Ag BMs/ePI (ii) maintained stable morphology endowed by the embedded structure and bundle micromesh construction of Ag NWs. **e**  $\Delta R/R_0$  vs. annealing time for Ag RNs/PIs and Ag BMs/PIs electrodes in air and  $N_2$  atmosphere, respectively. It is clearly that the bundle micromesh construction contributes for higher temperature tolerance.

atmosphere) and 265 °C ( $N_2$  atmosphere), respectively. In sharp contrast, the reference samples of Ag RNs/PIs showed degradation of electrical performance at 205 °C (ambient atmosphere) and 225 °C ( $N_2$  atmosphere) after  $\sim 30$  min (Fig. 2e), respectively. When the Ag NWs were embedded in PI matrix, the Ag BMs/ePI also exhibited higher temperature tolerance and thermal degradation temperature than Ag RNs/ePI electrode (Fig. 2a, b, Supplementary Fig. 4d). These results confirmed that the bundle micromesh structure helps to protect Ag NWs against high temperature. For the melting point of nanowires, a good estimate is obtained by the formula<sup>40</sup>:  $T_{mw} = T_{mb} \frac{1-4d}{3D}$ , where  $T_{mw}$  and  $T_{mb}$  is the melting point of the nanowires and the bulk material,  $d$  and  $D$  is the diameter of atom and wire, respectively. Based on this formula, it implies that the Ag NWs with larger diameter have smaller surface-area-to-volume ratio and lower surface energy, leading to higher thermal stability at evaluated temperature<sup>20,41</sup>. For random Ag NWs networks electrode, these nanowires dispersed separately with thin diameter. While for the Ag BMs electrode, these compact bundles were composed of aligned nanowires, which could be equivalent to larger diameter nanowires. Therefore, compared with random Ag NWs networks electrode, the Ag BMs electrode exhibited higher thermal stability in both  $N_2$  and ambient atmospheres (Fig. 2).

To further verify the role of bundle micromesh construction on the temperature resistance enhancement, different sheet resistance ( $\sim 10 \text{ ohm sq}^{-1}$ ,  $\sim 50 \text{ ohm sq}^{-1}$ ,  $\sim 100 \text{ ohm sq}^{-1}$ ) of Ag BMs/ePI electrodes (Fig. 3a, b), which corresponded to different Ag NWs bundle diameters (Fig. 3c–e), were prepared by tuning the Ag NWs dosage during spray coating process and checked at high temperature. It is clearly that the lower sheet resistance of Ag BMs/ePI electrode, which had larger bundle diameter, possessed

higher thermal stability under the same conditions (Fig. 3). As a typical example, the Ag BMs/ePI electrode ( $R_s$ ,  $\sim 10 \text{ ohm sq}^{-1}$ ; bundle diameter,  $\sim 1.5 \mu\text{m}$ ) could keep conductivity in both ambient (350 °C) and  $N_2$  (370 °C) atmospheres more than 1.5 h, while the control electrodes with sheet resistance of  $\sim 50 \text{ ohm sq}^{-1}$  (bundle diameter,  $\sim 0.5 \mu\text{m}$ ) and  $\sim 100 \text{ ohm sq}^{-1}$  (bundle diameter,  $\sim 0.3 \mu\text{m}$ ) failed quickly (Fig. 3a, b). Therefore, both conductivity and thermal stability of Ag BMs electrode can be tuned by controlling Ag NWs bundle diameters. The other more important advantages of the embedded Ag BMs structure are the ambient stability, chemical and mechanical robustness. The ambient stability of Ag BMs/ePI electrode was evaluated as a function of shelf life in air (relative humidity of 60% at room temperature). As shown in Fig. 4a, the sheet resistance of control sample Ag BMs/PIs dramatically increased from 10 to 156  $\text{ohm sq}^{-1}$  after 50 days, while there was only little increase in sheet resistance for Ag BMs/ePI ( $R_s$ ,  $\sim 10 \text{ ohm sq}^{-1}$ ) electrode after 8 months. The PI encapsulation layer would effectively block the permeation of moisture, oxygen, and sulfide in air which would accelerate degradation of Ag NWs, and thereby enhanced the ambient stability. The burying of the Ag BMs electrode in PI matrix also can well protect it from chemical corrosion, including organic solvents and corrosive acid-base solutions. As shown in Fig. 4b, the Ag BMs/ePI can maintain conductivity after 1 h immersion in different solvents, such as deionized water, isopropyl alcohol, ethanol, acetone, and toluene. The little decrease in sheet resistance stemmed from the fact that some impurities (e.g., Ag nanoparticles, disconnected Ag NWs, contaminants or surfactants) on the Ag BMs surface were washed away by solvents<sup>42</sup>. Even the Ag BMs/ePI electrode were immersed in acidic and alkaline

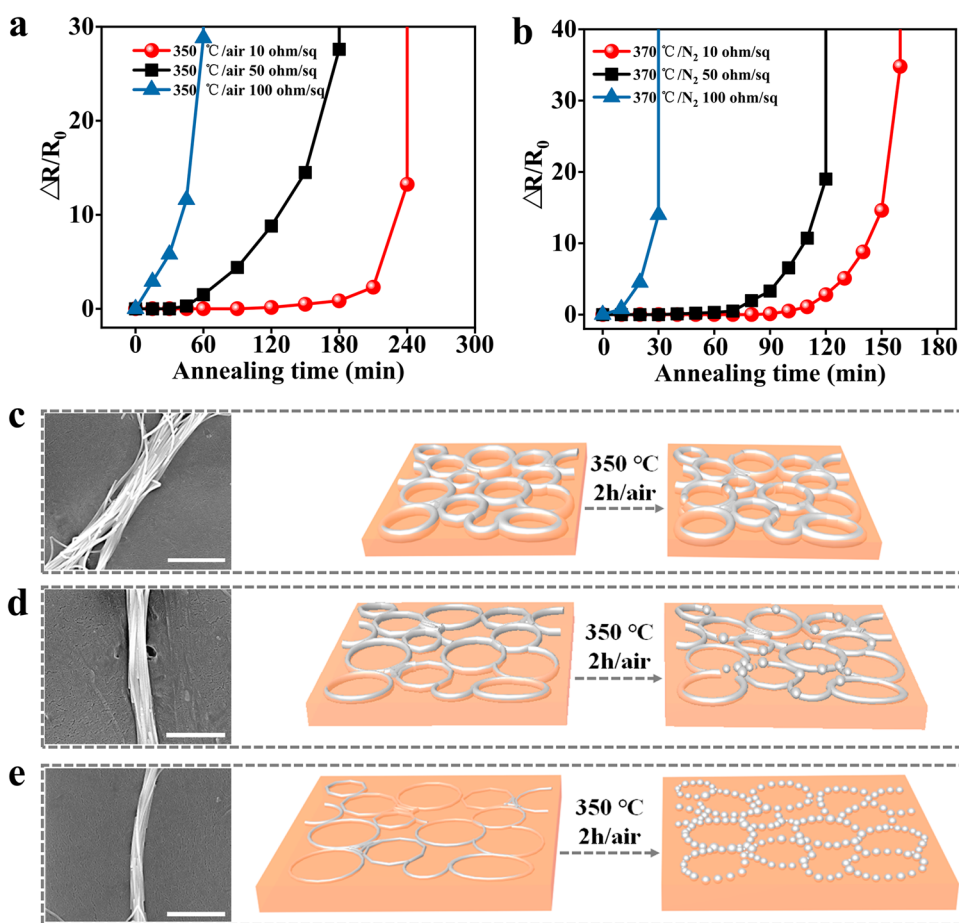


**Fig. 3 Thermal stability of the Ag BMs/ePI electrode with different  $R_s$  values.** The Ag BMs/ePI electrode with different  $R_s$  values in nitrogen **a** and air **b** conditions, respectively. **c–e** SEM images of Ag BMs/ePI electrodes with different bundle diameters, corresponding to the  $R_s$  of **c**  $\sim 10$  ohm  $\text{sq}^{-1}$ , **d**  $\sim 50$  ohm  $\text{sq}^{-1}$ , and **e**  $\sim 100$  ohm  $\text{sq}^{-1}$  and the corresponding schematic diagram for morphological evolution in ambient atmosphere at high temperature of 350 °C. The scale bars in **c**, **d** and **e** were 2  $\mu\text{m}$ .

solution with different pH values for 1 h (Fig. 4c), there were still no obvious increase in the sheet resistance, enabling a reliable conducting film in harsh conditions for different practical applications.

In addition, different types of external damages (e.g., delamination, scratch, crack) would be caused on the flexible electrodes due to the harsh processing environment in manufacturing process, therefore, mechanical durability is another important concern for highly reliable devices fabrication. As shown in Fig. 4d, a mechanical adhesion test with 3 M scotch 600 tape was performed on Ag BMs/ePI electrode to assess its durability. The sheet resistance change of Ag BMs/ePI electrode was less than 1% after 1000 times adhesion test cycles. While for the control sample of Ag BMs/PIs electrode, it can be detached from the substrate only after 1 cycle (Supplementary Fig. 5a) and therefore was intolerant to scratch due to the weak bonding force between Ag BMs and PI surface. On the other hand, the cyclic bending test was conducted to evaluate the mechanical reliability using a bending fatigue test. The Ag BMs/ePI electrode can maintain a stable conductivity ( $\Delta R/R_0 < 2\%$ ) even after 10,000 cycles with 1.5 mm bending radius under tensile and compressive modes (Fig. 4e), and was therefore suitable for high-reliability flexible electronics application. In contrast, the commercial flexible transparent ITO/PET electrode ( $R_s$ ,  $\sim 11$  ohm  $\text{sq}^{-1}$ ) performance degraded quickly after several bending cycles (Supplementary Fig. 5b). Moreover, the Ag BMs/ePI electrode resistance change was monitored in real-time with 1.5 mm curvature radius, which kept stable throughout the bending process and maintained the lighted

LEDs with consistent brightness (Fig. 4f and Supplementary Movie 1). In addition, the resistance of the Ag BMs/ePI electrode also can keep stable throughout the whole bending process in different directions (Supplementary Fig. 6 and Movie 2), indicating the directional flexibility of the Ag BMs/ePI electrode. The remarkable mechanical reliability of Ag BMs/ePI electrode resulted from its embedded bundle micromesh structure, where the Ag BMs were fixed strongly by PI matrix with a stable interconnection to accommodate different extreme mechanical deformations. Therefore, the flexible transparent Ag BMs/ePI electrode can endow with good environmental adaptivity of thermal, chemical, and mechanical stimuli, promising for multi-scenario applications.

#### Heating performance of Ag BMs/ePI electrical heater

The potential capability of Ag BMs/ePI as flexible transparent electrode platform was demonstrated by fabricating an electrical heater, which had been used to control the temperature in different devices, including heating systems in the industry, defogging mirrors and windows in car, personal thermal management for arthritis and cancer<sup>43–45</sup>. Due to the inelastic collisions between accelerated phonons and electrons, the Joule heat will be generated in the conductive materials when the current passes through<sup>44</sup>. The thermal stability and mechanical robustness of Ag BMs/ePI electrode are critical for high-performance heater design (Fig. 5a). As shown in Fig. 5b, the steady-state saturation temperature ( $T_s$ ) of Ag BMs/ePI heater ( $R_s \sim 10$  ohm  $\text{sq}^{-1}$ , 2 cm  $\times$  2 cm) increased with the supplied bias increase as more Joule heat

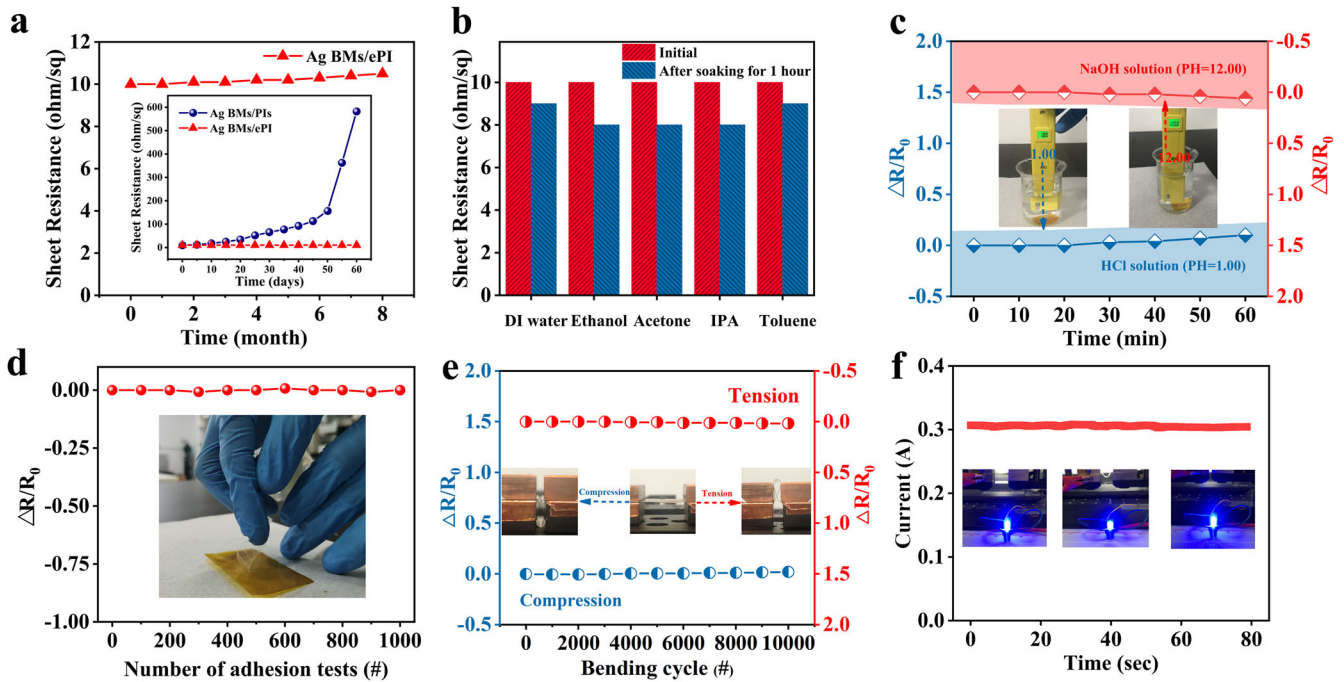


**Fig. 4 Stability of the Ag BMs/ePI electrode.** **a** Sheet resistance change of the Ag BMs/ePI and Ag BMs/PIs exposure to air at room temperature. **b** Chemical stability of Ag BMs/ePI electrode in different solvents for 1 h, including deionized water, isopropyl alcohol, ethanol, acetone, and toluene. **c** Chemical stability of Ag BMs/ePI electrodes in acid (HCl, pH = 1.0) and alkaline (NaOH, pH = 12.0) solutions for 1 h. **d** Adhesion test of Ag BMs/ePI electrode by using 3 M scotch 600 tape. **e** Sheet resistance change of Ag BMs/ePI conducting film as a function of the number of tensile and compressive bending with curvature radius of 1.5 mm. Insets showed the demonstration of electrode bend in tension and compression modes. **f** Real-time monitoring of the resistance changes of Ag BMs/ePI electrode during bending process. Insets were the photographs of stable LED lighting connected to the electrode.

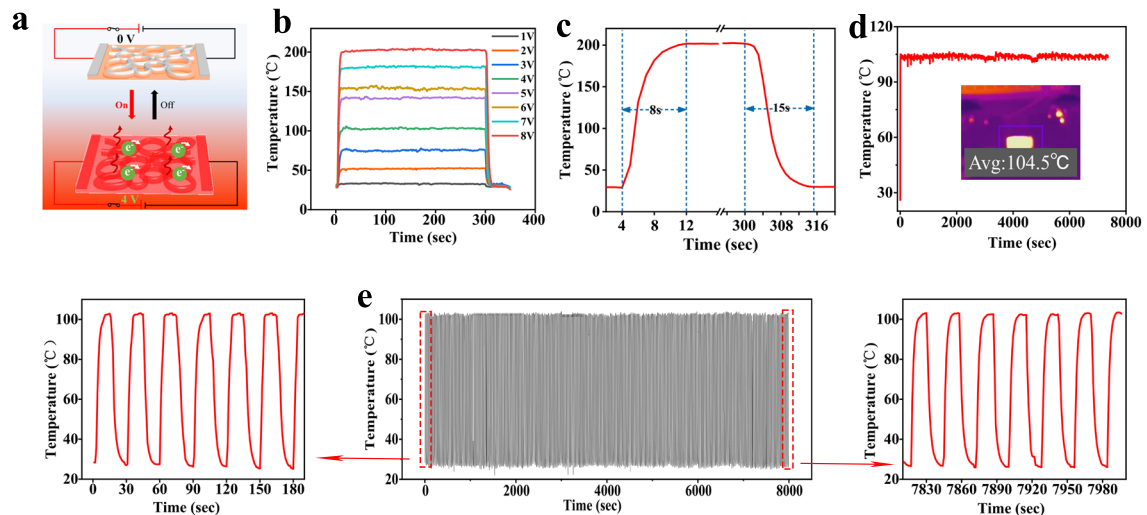


**Fig. 5 Heating characteristics of the Ag BMs/ePI electrode.** **a** Schematic diagram for the heating and cooling process for Ag BMs/ePI heater. **b** Time-dependent surface temperature of the flexible transparent Ag BMs/ePI heater ( $R_s \sim 10 \text{ ohm sq}^{-1}$ ,  $2 \text{ cm} \times 2 \text{ cm}$ ) with different supplied voltages. **c** Response and cooling time of the Ag BMs/ePI heater at 8 V constant voltage. **d** Long-term time-dependent surface temperature of the Ag BMs/ePI heater at 4 V. Inset was the IR camera image of the real device. **e** Heating stability and repeatability of the Ag BMs/ePI heater at 4 V, corresponding to the first 6 cycles (left) and the last 6 cycles (right).

power was generated, and a  $T_s$  of  $\sim 204.3^\circ\text{C}$  can be obtained at low bias of 8 V. Especially, the Ag BMs/ePI heater can be rapidly heated to the saturated temperature within 8 s and naturally cooled down to room temperature within 15 s after power off (Fig. 5c), demonstrating the promising applications in fast heating and cooling required flexible transparent film heaters. The overall performance of Ag BMs/ePI heater is comparable or superior to other important works on high-quality heaters with different

conducting materials (Supplementary Table 1). For the Ag BMs/ePI heater, due to the Biot number ( $Bi$ ) was much less than 1 (see the  $Bi$  calculation in the Supplementary Information), the temperature rise of the heater is determined by the applied voltage, the resistance of heater, and the surface heat transfer coefficient<sup>46</sup>. Therefore, for a fixed Ag BMs/ePI heater, based on the equation 1:  $T_s = T_0 + \frac{U^2}{RhA}$  ( $T_s$ : saturation temperature,  $T_0$ : initial ambient temperature,  $U$ : supplied voltage,  $R$ : resistance of the heater,

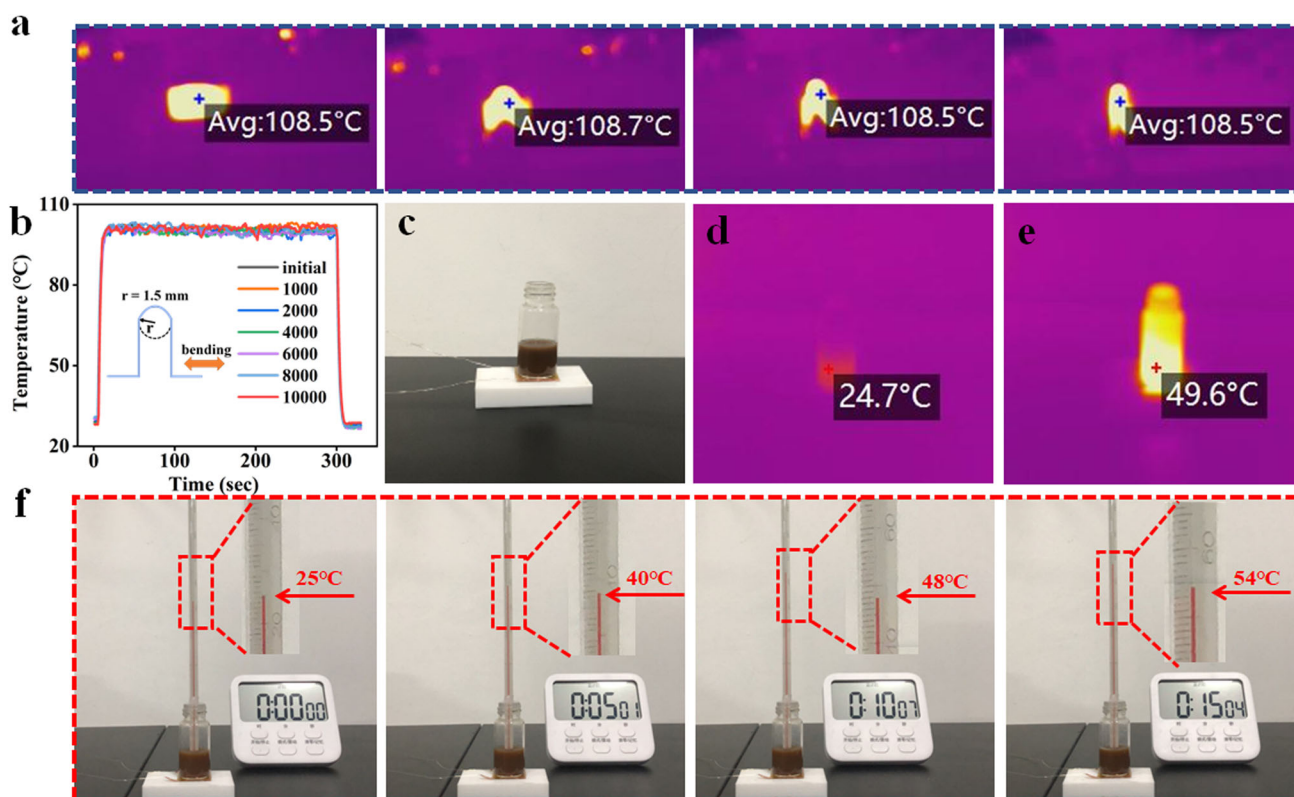


**Fig. 6** IR camera and digital images of the Ag BMs/ePI heater. **a** IR camera images of the Ag BMs/ePI heater upon different bending radius. **b** Cyclic electrical heating performance of Ag BMs/ePI heater at 4V while being bent repeatedly to 1.5 mm diameter. After 10000 bending cycles, it still maintained stable performance. **c–e** Digital and IR camera images of the Ag BMs/ePI heater in coffee heating with supplied voltage of 4 V. **f** Digital images of the Ag BMs/ePI heater in coffee heating at 4 V.

$h$ : convective heat transfer coefficient,  $A$ : area of the heater)<sup>43</sup>, the  $T_s$  was mainly determined by the supplied voltage, which increased with the supplied voltage (Fig. 5b). On the other hand, to understand the mechanism of the rapid thermal response behavior of Ag BMs/ePI heater, a good estimate for response time of Ag NWs-based heater is obtained by the equation 2:  $t = \frac{\rho d c}{h}$ , where  $t$  is the response time,  $\rho$ ,  $d$ ,  $c$ , and  $h$  is the density, thickness, specific heat capacity, convective heat transfer coefficient of the substrate, respectively<sup>47</sup>. As shown in Supplementary Fig. 7a, the saturation temperature was independent on the substrate thickness, and the response time was proportional to the PI substrate thickness. As shown in Supplementary Fig. 7b, the response time of Ag BMs/ePI heaters became shorter from 16 s to 6 s with PI thickness decrease from  $\sim 260 \mu\text{m}$  to  $\sim 50 \mu\text{m}$ . It is worth to note that although the Ag BMs/ePI can withstand high temperature of  $\sim 350^\circ\text{C}$  at an ambient atmosphere (Fig. 2a), the Ag BMs/ePI heater cannot achieve this saturation temperature under electrical stress. Different from the thermal breakdown only induced by external heat sources, electromigration (electrical breakdown) mainly accounts for the failure of Ag BMs/ePI heater under electrical stress, accompanied with the driving force of Joule heating for nanowires failure<sup>22,48</sup>. In Ag BMs/ePI heater, the electrical current may not flow identically in all network locations, leading to higher temperature in localized hotspots with high current densities and lower thermal stability<sup>49</sup>. However, compared with the random Ag NWs networks embedded in PI (Ag RNs/ePI) heater, the Ag BMs/ePI heater exhibited high performance in terms of the maximum  $T_s$  and homogenous temperature distribution. As shown in Supplementary Fig. 8, the maximum  $T_s$  of Ag RNs/ePI heater only can achieve  $138.8^\circ\text{C}$  ( $\sim 10 \text{ ohm sq}^{-1}$ ,  $2 \text{ cm} \times 2 \text{ cm}$ ) which was obvious lower than  $\sim 204.3^\circ\text{C}$  of the ordered Ag BMs/ePI heater (Fig. 5b). In addition, the mean saturation

temperature of Ag BMs/ePI heater was  $103.7 \pm 1.2^\circ\text{C}$ , while the mean temperature of random Ag NWs/ ePI heater was  $100.5 \pm 8.5^\circ\text{C}$ . It is clearly that the heat distribution of the Ag BMs/ePI heater ( $6 \text{ cm} \times 6 \text{ cm}$ ) was more homogenous over the entire film due to the uniform resistance distribution. To satisfy the reliability requirement in practical application for Ag BMs/ePI heater, long-term working stability is another concern. As shown in Fig. 5d, this flexible transparent heater exhibited an extremely stable surface temperature of  $\sim 103.7 \pm 1.2^\circ\text{C}$  within 2 h with 4 V operation voltage as a representative. Upon the repeated operation voltage of 4 V, Ag BMs/ePI heater exhibited 240 steady heating and cooling cycles within 2 h (Fig. 5e), indicating the sufficient repeatability and remarkable heating stability of Ag BMs/ePI heater in real application.

On the other hand, to demonstrate the stability of flexible Ag BMs/ePI heater subjected to bending, the surface temperature was recorded. As shown in Fig. 6a, the flexible electrical heater ( $2.5 \text{ cm} \times 2 \text{ cm}$ ) upon different bending radius ( $r$ ,  $\infty$ ,  $\sim 10 \text{ mm}$ ,  $\sim 3 \text{ mm}$ ,  $\sim 1.5 \text{ mm}$ ) exhibited a stable and uniform temperature distribution. Furthermore, this flexible transparent Ag BMs/ePI heater working at 4 V can survive upon repeated bending ( $r = 1.5 \text{ mm}$ ) with nearly overlapped temperature curves after the 1st, 1000th, 2000th, 4000th, 6000th, 8000th and 10,000th cycles (Fig. 6b). These results confirmed the good mechanical stability and long service life of Ag BMs/ePI electrical heater in wearable electronics applications. The rapid thermal response and low driving voltage indicate that the Ag BMs/ePI heater can achieve desired temperature rapidly and is safe for the human body. Due to the wide heating temperature range (room temperature to  $\sim 204^\circ\text{C}$ , Fig. 5b), the Ag BMs/ePI heater can be widely applied for such as heating water outdoors, deicing in icy and snowy weather, thermotherapy ( $40\text{--}50^\circ\text{C}$ ) and keeping warm ( $40\text{--}60^\circ\text{C}$ ). As shown

in Fig. 6c–f and Supplementary Movie 3, Ag BMs/ePI heater (2 cm × 2 cm) was placed to the bottom of a glass container to heat coffee (5 mL), and the coffee temperature was monitored in real-time by a mercury thermometer. When 4 V bias voltage was applied, the heat produced from Ag BMs/ePI heater with surface temperature of ~104 °C was efficiently transferred to coffee. After heating for 300 s and 900 s, the coffee temperature can be raised quickly from initial 25 °C to 40 °C and 54 °C respectively, which meets the drinking temperature (Fig. 6f). Due to the ultra-flexibility, this heater can also be wrapped around the side wall of a container for heating. In view of the extraordinary performance, as a typical example, the portable flexible Ag BMs/ePI heater can be used to melt the snow and ice, or heat the cold water and food for solving diet problem when people execute tasks in cold places. In addition, Ag BMs/ePI film can be employed as thermochromic display device in combination with thermochromic inks (Supplementary Fig. 9, Movie 4). The color of predetermined patterns on Ag BMs/ePI can be tuned by choosing different operation voltages and thermochromic inks, implying that complicated color-changing paints can be achieved for other applications such as anti-fake and art show. These results mentioned above indicate that this high-temperature tolerance, chemical and mechanical robustness flexible transparent Ag BMs/ePI electrode has promising potential in future applications in terms of heating system, wearable device, intelligent robot, heat-resisting electronics, and so on. For special applications that require large area, the scalability of the conducting film is a major concern. It is worth mentioning that the large Ag BMs/ePI film fabrication can be guaranteed *via* facile spray coating and transfer method which does not have the problem of area restriction provided by other conventional fabrication equipment.

In summary, a high performance flexible transparent Ag BMs/ePI electrode has been fabricated *via* facile, low-cost and scale-up spray coating and transfer method. The well-organized Ag NWs bundle micromesh can be equivalent to stable nanowires with larger diameter, and the encapsulation with PI matrix can effectively suppress the surface diffusion of Ag atoms and prevent chemical corrosion. Therefore, the synergistic effect of bundle micromesh construction and embedded structure in Ag BMs/ePI electrode render the high-temperature tolerance in air (370 °C, ~90 min) and N<sub>2</sub> (400 °C, ~60 min) atmospheres, which also result in uniform sheet resistance distribution, high chemical stability, low surface roughness, good mechanical and optoelectrical performance. As proof of viability, a flexible transparent Ag BMs/ePI heater was fabricated, which can generate high saturation temperature up to 204 °C with long-term stability and rapid heating response. Even under extreme bending stimuli ( $r = 1.5$  mm), the Ag BMs/ePI heater still can maintain heating performance without degradation after 10,000 cycles. The study paves the way for environment adaptable conducting film preparation with different metal nanowires (e.g., Cu NWs, Ag NWs, Au NWs), rendering wider applications in flexible transparent optoelectronics devices.

## METHODS

### PDMS preparation

The PDMS (Sylgard 184, Dow Corning) substrate with thickness of ~200 μm was fabricated by mixing the PDMS curer and base at a weight ratio of 1:10, and cured at 80 °C for 4 h.

### Ag BMs/ePI electrode preparation

Ag NWs (~30 nm diameter, ~20 μm length, XF NANO Co., LTD.) ink (0.5 mg ml<sup>-1</sup>) with isopropanol solvent was spray-coated on PDMS substrate, then polyimide solution (DuPont SP-21, Aladdin) was spin-coated to encapsulated Ag NWs. Finally, the fresh samples were placed in a vacuum oven to solidify the polyimide solution at 100 °C for 1 h. Finally, the cured PI film (~70 μm thick) was peeled off from the substrate to obtain the desired Ag BMs/ePI electrode.

## Thermochromic display device preparation

The thermochromic inks (Sinopharm Chemical Reagent Co., LTD) with different colors (black, red, blue) were coated onto Ag BMs/ePI surface directly.

## Characterizations

Optical microscope (MX6R, Sunny Optical Technology Co., LTD), SEM (Nova NanoSEM 450) and atomic force microscopy (AFM) system (Nano Wizard 4, JPK) were employed to reveal the Ag BMs morphology. Transmittance and sheet resistance measurements for Ag BMs conducting film were performed on an UV-vis spectrometer (TU-1901, Beijing General Analytical Instrument) and a portable four-probe meter (M-3 portable four-probe meter, China), respectively. The tubular furnace (OTF-1200X, HF-kejing) was employed for the thermal stability measurement of Ag NWs electrodes. Thermogravimetric analysis (TGA, DSC2500, TA Instruments) were performed to verify the stability of polyimide samples with heating rate at 10 °C min<sup>-1</sup> in N<sub>2</sub> condition at flow rate of 100 ml min<sup>-1</sup>. The surface temperature of Ag BMs/ePI heater was recorded using thermal infrared camera (D-384M, Guide Infrared Co., Ltd.). A digital multimeter (Agilent B2900) was used to examine the resistance change and supply bias for Ag BMs/ePI electrode.

## DATA AVAILABILITY

The data that support the findings of this study are available from the corresponding author upon reasonable request.

Received: 20 January 2022; Accepted: 22 May 2022;

Published online: 20 June 2022

## REFERENCES

- Li, N. et al. Large-scale flexible and transparent electronics based on monolayer molybdenum disulfide field-effect transistors. *Nat. Electron.* **3**, 711–717 (2020).
- Ji, C. G., Liu, D., Zhang, C. & Guo, L. J. Ultrathin-metal-film-based transparent electrodes with relative transmittance surpassing 100%. *Nat. Commun.* **11**, 3376 (2020).
- Peng, J. et al. Surface coordination layer passivates oxidation of copper. *Nature* **586**, 390 (2020).
- Datta, R. S. et al. Flexible two-dimensional indium tin oxide fabricated using a liquid metal printing technique. *Nat. Electron.* **3**, 51–58 (2020).
- Sharma, V., Koivikko, A., Yiannacou, K., Lahtonen, K. & Sariola, V. Flexible biodegradable transparent heaters based on fractal-like leaf skeletons. *npj Flex. Electron.* **4**, 27 (2020).
- Chen, D. et al. Thermally stable silver nanowire-polyimide transparent electrode based on atomic layer deposition of zinc oxide on silver nanowires. *Adv. Funct. Mater.* **25**, 7512–7520 (2015).
- Xiong, J. Q. et al. A deformable and highly robust ethyl cellulose transparent conductor with a scalable silver nanowires bundle micromesh. *Adv. Mater.* **30**, 1802803 (2018).
- Hsu, P. C. et al. Performance enhancement of metal nanowire transparent conducting electrodes by mesoscale metal wires. *Nat. Commun.* **4**, 2522 (2013).
- Kang, S. et al. Transparent and conductive nanomembranes with orthogonal silver nanowire arrays for skin-attachable loudspeakers and microphones. *Sci. Adv.* **4**, eaas8772 (2018).
- Jung, D. et al. Highly conductive and elastic nanomembrane for skin electronics. *Science* **373**, 1022–1026 (2021).
- Xue, J. et al. Nanowire-based transparent conductors for flexible electronics and optoelectronics. *Sci. Bull.* **62**, 143–156 (2017).
- Han, S. et al. Nanorecycling: Monolithic integration of copper and copper oxide nanowire network electrode through selective reversible photochemical reduction. *Adv. Mater.* **27**, 6397–6403 (2015).
- Kim, D. et al. A transparent and flexible capacitive-force touch pad from high-aspect-ratio copper nanowires with enhanced oxidation resistance for applications in wearable electronics. *Small Methods* **2**, 1800077 (2018).
- Ding, S., Tian, Y. H., Jiu, J. T. & Sugauma, K. Highly conductive and transparent copper nanowire electrodes on surface coated flexible and heat-sensitive substrates. *RSC Adv.* **8**, 2109–2115 (2018).
- Han, S. et al. Transparent air filters with active thermal sterilization. *Nano Lett.* **22**, 524–532 (2022).
- Jin, J. et al. High-performance hybrid plastic films: A robust electrode platform for thin-film optoelectronics. *Energ. Environ. Sci.* **6**, 1811–1817 (2013).



17. Zeng, X. Y., Zhang, Q. K., Yu, R. M. & Lu, C. Z. A new transparent conductor: Silver nanowire film buried at the surface of a transparent polymer. *Adv. Mater.* **22**, 4484–4488 (2010).
18. Spechler, J. A., Koh, T.-W., Herb, J. T., Rand, B. P. & Arnold, C. B. A transparent, smooth, thermally robust, conductive polyimide for flexible electronics. *Adv. Funct. Mater.* **25**, 7428–7434 (2015).
19. Im, H. G. et al. Flexible transparent conducting hybrid film using a surface-embedded copper nanowire network: A highly oxidation-resistant copper nanowire electrode for flexible optoelectronics. *ACS Nano* **8**, 10973–10979 (2014).
20. Khaligh, H. H. & Goldthorpe, I. A. Failure of silver nanowire transparent electrodes under current flow. *Nanoscale Res. Lett.* **8**, 235 (2013).
21. Song, T. B. et al. Nanoscale joule heating and electromigration Enhanced ripening of silver nanowire contacts. *ACS Nano* **8**, 2804–2811 (2014).
22. Patil, J. J. et al. Failing forward: Stability of transparent electrodes based on metal nanowire networks. *Adv. Mater.* **33**, 2004356 (2021).
23. Lee, J.-Y., Connor, S. T., Cui, Y. & Peumans, P. Solution-processed metal nanowire mesh transparent electrodes. *Nano Lett.* **8**, 689–692 (2008).
24. Kim, A., Won, Y., Woo, K., Kim, C. H. & Moon, J. Highly transparent low resistance ZnO/Ag nanowire/ZnO composite electrode for thin film solar cells. *ACS Nano* **7**, 1081–1091 (2013).
25. Im, H. G. et al. Flexible transparent conducting composite films using a monolithically embedded AgNW electrode with robust performance stability. *Nanoscale* **6**, 711–715 (2014).
26. Alotaibi, F., Tung, T. T., Nine, M. J., Coghlan, C. J. & Losic, D. Silver nanowires with pristine graphene oxidation barriers for stable and high performance transparent conductive films. *ACS Appl. Nano Mater.* **1**, 2249–2260 (2018).
27. Song, T.-B. et al. Highly robust silver nanowire network for transparent electrode. *ACS Appl. Mater. Interfaces* **7**, 24601–24607 (2015).
28. Ding, Y., Cui, Y., Liu, X., Liu, G. & Shan, F. Welded silver nanowire networks as high-performance transparent conductive electrodes: welding techniques and device applications. *Appl. Mater. Today* **20**, 100634 (2020).
29. Giusti, G. et al. Thermal annealing effects on silver nanowire networks. *Int. J. Nanotechnol.* **11**, 785–795 (2014).
30. Liang, C., Sun, X. Y., Su, W. M., Hu, Y. W. & Duan, J. A. Fast welding of silver nanowires for flexible transparent conductive film by spatial light modulated femtosecond laser. *Adv. Eng. Mater.* **23**, 2100584 (2021).
31. Park, J. H. et al. Plasmonic-tuned flash Cu nanowelding with ultrafast photochemical-reducing and interlocking on flexible plastics. *Adv. Funct. Mater.* **27**, 1701138 (2017).
32. Huang, Y. L. et al. Self-limited nanosoldering of silver nanowires for high-performance flexible transparent heaters. *ACS Appl. Mater. Interfaces* **11**, 21850–21858 (2019).
33. Hwang, B., Shin, H. A. S., Kim, T., Joo, Y. C. & Han, S. M. Highly reliable Ag nanowire flexible transparent electrode with mechanically welded junctions. *Small* **10**, 3397–3404 (2014).
34. Sannicolo, T. et al. Electrical mapping of silver nanowire networks: A versatile tool for imaging network homogeneity and degradation dynamics during failure. *ACS Nano* **12**, 4648–4659 (2018).
35. Sharma, V. et al. Performance comparison of fast, transparent, and biotic heaters based on leaf skeletons. *Adv. Eng. Mater.* 2101625 (2022).
36. Suh, Y. D. et al. Random nanocrack, assisted metal nanowire-bundled network fabrication for a highly flexible and transparent conductor. *RSC Adv.* **6**, 57434–57440 (2016).
37. Xiong, J. et al. A tailorable spray-assembly strategy of silver nanowires-bundle mesh for transferable high-performance transparent conductor. *Adv. Funct. Mater.* **31**, 2006120 (2021).
38. Jia, Y. et al. Silver nanowire transparent conductive films with high uniformity fabricated via a dynamic heating method. *ACS Appl. Mater. Interfaces* **8**, 9865–9871 (2016).
39. Singh, M. et al. Silver nanowires binding with sputtered ZnO to fabricate highly conductive and thermally stable transparent electrode for solar cell applications. *ACS Appl. Mater. Interfaces* **8**, 12764–12771 (2016).
40. Gordon, E. B., Karabulin, A. V., Matyushenko, V. I. & Khodos, I. I. Experimental study of thermal stability of thin nanowires. *J. Phys. Chem. A* **119**, 2490–2501 (2015).
41. Zhang, J. H., Fu, Q. S., Cui, Z. X. & Xue, Y. Q. Size-dependent melting thermodynamic properties of selenium nanowires in theory and experiment. *CrytEngComm* **21**, 430–438 (2019).
42. Guo, X. Y. et al. Silver nanowire/polyimide composite transparent electrodes for reliable flexible polymer solar cells operating at high and ultra-low temperature. *RSC Adv.* **5**, 24953–24959 (2015).
43. Ma, Z. L. et al. High-performance and rapid-response electrical heaters based on ultraflexible, heat-resistant, and mechanically strong aramid nanofiber/Ag nanowire nanocomposite Papers. *ACS Nano* **13**, 7578–7590 (2019).
44. Zhang, L. S., Baima, M. & Andrew, T. L. Transforming commercial textiles and threads into sewable and weavable electric heaters. *ACS Appl. Mater. Interfaces* **9**, 32299–32307 (2017).
45. Shi, M. et al. Ti<sub>3</sub>C<sub>2</sub>T<sub>x</sub> MXene-decorated nanoporous polyethylene textile for passive and active personal precision heating. *ACS Nano* **15**, 11396–11405 (2021).
46. Kwak, H. S., Kim, K., Shon, B. C., Lee, H. & Han, C. S. Thermal characteristics of a transparent film heater using single-walled carbon nanotubes. *J. Nanosci. Nanotechnol.* **10**, 3512–3515 (2010).
47. Ji, S. L., He, W. W., Wang, K., Ran, Y. X. & Ye, C. H. Thermal response of transparent silver nanowire/PEDOT:PSS film heaters. *Small* **10**, 4951–4960 (2014).
48. Zhao, J. O., Sun, H. Y., Dai, S., Wang, Y. & Zhu, J. Electrical breakdown of nanowires. *Nano Lett.* **11**, 4647–4651 (2011).
49. Khaligh, H. H. et al. The joule heating problem in silver nanowire transparent electrodes. *Nanotechnology* **28**, 425703 (2017).

## ACKNOWLEDGEMENTS

This work is supported by the Guangdong Basic and Applied Basic Research Foundation program (Grant No. 2020A1515110292), Shandong Provincial Natural Science Foundation (Grant No. ZR2020QF080), and Qilu Young Scholar program (Grant No. 11500089963022), China. Additional discussions about the detail of the SEM images of Ag BMs/ePI electrode with multi-level resolutions at different magnifications, Ag BMs/ePI conductor sheet resistance distribution, haze, thermal stability at 350 °C in nitrogen atmosphere, Ag BMs on PDMS substrate characteristics, thermo-chromic process of Ag BMs/ePI electrode, comparison of key performance parameters between Ag BMs/ePI heater with other different important heaters and calculation formula of Bi are included. This material is available free of charge via the Internet at <https://doi.org/xxxxxxxxxx>.

## AUTHOR CONTRIBUTIONS

K.Q. and J.X. conceived and designed the work. B.S. carried out conformable device fabrication and performed electrical and optical measurements. B.S., R.X., and W.H. conducted the electric heating test. K.Q., J.X., J.C., B.S., and R.X. wrote and revised the manuscript. B.S., R.X., X.H., J.X., W.H., Y.X., Z.F., H.Z., and X.S. analyzed and interpreted the data. All authors discussed the results and commented on the final manuscript. K. Q., J.X., J.C., J.W., and P.C. supervised the project.

## COMPETING INTERESTS

The authors declare no competing interests.

## ADDITIONAL INFORMATION

**Supplementary information** The online version contains supplementary material available at <https://doi.org/10.1038/s41528-022-00182-8>.

**Correspondence** and requests for materials should be addressed to Jingjing Chang, Jiaqing Xiong or Kai Qian.

**Reprints and permission information** is available at <http://www.nature.com/reprints>

**Publisher's note** Springer Nature remains neutral with regard to jurisdictional claims in published maps and institutional affiliations.



**Open Access** This article is licensed under a Creative Commons Attribution 4.0 International License, which permits use, sharing, adaptation, distribution and reproduction in any medium or format, as long as you give appropriate credit to the original author(s) and the source, provide a link to the Creative Commons license, and indicate if changes were made. The images or other third party material in this article are included in the article's Creative Commons license, unless indicated otherwise in a credit line to the material. If material is not included in the article's Creative Commons license and your intended use is not permitted by statutory regulation or exceeds the permitted use, you will need to obtain permission directly from the copyright holder. To view a copy of this license, visit <http://creativecommons.org/licenses/by/4.0/>.